

# Direct Observations of Surface-Wave Eigenfunctions at the Homestake 3D Array

Patrick Meyers,<sup>1</sup> Tanner Prestegard,<sup>1</sup> Daniel C. Bowden,<sup>2</sup>  
Victor C. Tsai,<sup>2</sup> Vuk Mandic,<sup>1</sup> Gary Pavlis,<sup>3</sup> and Ross Caton<sup>3</sup>

*<sup>1</sup>School of Physics and Astronomy, University of Minnesota,  
Minneapolis, Minnesota 55455, USA*

*<sup>2</sup>Seismological Laboratory, California Institute of Technology, Pasadena, CA 91125, USA*

*<sup>3</sup>Department of Geological Sciences,  
Indiana University, Bloomington, IN 47405, USA*

## Abstract

(add abstract)

Surface wave background, motivation for observations

Direct observations of eigenfunctions

Inversions consistent with expectation

Implications in broader context

PACS numbers:

## I. INTRODUCTION

Introduction to surface waves, long history, use

Discussion of lack of observations at depth. Even though borehole arrays exist, no clear confirmation of expected surface-wave behavior as yet.

(The above 2 points should probably be somewhat substantial, e.g. > 1 page total)

Brief intro to accomplishments of the paper

## II. METHODS

### A. Observational Methods

We use transient seismic events to measure the surface-wave eigenfunctions. ([text from Gary/Ross on how picking is done, direction/blast time is estimated. Maybe plot of transient events]).

For each transient event, we rotate from East West/North South coordinates to radial and transverse coordinates. We then plot the waveform and a frequency-time map of the phase delay between the radial and vertical channels for each event for several surface stations. We identify times and frequencies when the radial-to-vertical phase is consistent with retrograde motion, which indicates that surface-waves are the dominant component of the seismic field. We define the radial-to-vertical phase using the cross-correlation of radial and vertical channels

$$\phi_{RV}(f, t) = \arctan \left[ \frac{\text{Im} \left( \tilde{R}^*(f, t) \times \tilde{V}(f, t) \right)}{\text{Re} \left( \tilde{R}^*(f, t) \times \tilde{V}(f, t) \right)} \right]. \quad (1)$$

$\tilde{R}(f, t)$  indicates the Fourier transform of the radial data at frequency  $f$  for the time segment starting at time  $t$ .  $\tilde{V}(f, t)$  indicates the same for the vertical channel. The asterisk indicates complex conjugation, while “Im” indicates the imaginary part of the cross-correlation and “Re” indicates the real part. ([add figure with trace and ft-map? and/or location of mine blasts used? or table of dates, etc.?]).

We use 28 mine blasts observed by the Homestake seismometer array during July 2015. We have used the above prescription to identify which parts of the waveforms are dominated by surface waves. For each blast, we calculate as many discrete Fourier transforms of length

10 s as possible for each seismometer in the array. This leaves us with 0.1 Hz frequency resolution, and we restrict our observations to the frequency band from 0.4 – 1.2 Hz for both the radial and the vertical channels because this is the region of frequency space where most of the surface-wave power appears to be concentrated for these blasts. We refer to the radial data point at frequency,  $f$ , and time,  $t$ , in seismometer,  $i$ , located at depth,  $z_i$ , as  $\tilde{R}_i(f, t; z_i)$ , and the corresponding vertical data point as  $\tilde{V}_i(f, t; z_i)$ .

We are attempting to observe Rayleigh waves and so we only consider the part of the radial measurement that is consistent with retrograde motion. This means that we perform a projection of our data onto the phase angle consistent with retrograde motion **phrasing a bit awkward...**

$$\tilde{\mathcal{R}}_i(f, t; z_i) = -|\tilde{R}_i(f, t; z_i)| \times \text{Im } e^{i\phi_{RV}}. \quad (2)$$

In the above expression, vertical lines indicate modulus, and we use the minus sign to impose the condition that measurements consistent with retrograde motion are positive, while those consistent with prograde motion are negative.  $\tilde{\mathcal{R}}_i(f, t; z_i)$  is now a real-valued quantity.

We then normalize each data point by the average over radial surface station measurements of the corresponding time and frequency. That is

$$\hat{r}_i(f, t; z_i) = \frac{\tilde{\mathcal{R}}_i(f, t; z_i)}{\text{mean} \left[ \{ \tilde{\mathcal{R}}_j(f, t; 0) \text{ for } j \text{ where } z_j = 0 \} \right]} \quad (3)$$

$$\hat{v}_i(f, t; z_i) = \frac{|\tilde{V}_i(f, t; z_i)|}{\text{mean} \left[ \{ \tilde{\mathcal{R}}_j(f, t; 0) \text{ for } j \text{ where } z_j = 0 \} \right]} \quad (4)$$

In the above expressions,  $j$  runs over all stations positioned on the surface, and the minus sign on the vertical component is taken to be consistent with the convention in [1]. We remove measurements where  $\hat{r}_i(f, t; z_i)$  and  $\hat{v}_i(f, t; z_i)$  are greater than 1.5, as values this large indicate outliers whose amplitudes are much larger than the typical amplitude seen across the surface stations. This removes 15% of the individual data pixels.

Finally, we take the mean and variance across all times at each depth and each frequency. We indicate this with

$$\hat{r}(f, z) = \frac{1}{N_{t,z}} \sum_{i \text{ for } z_i=z} \sum_t \hat{r}_i(f, z_i; t) \quad (5)$$

$$\sigma_r^2(f, z) = \frac{1}{N_{t,z}} \sum_{i \text{ for } z_i=z} \sum_t (\hat{r}_i(f, z_i; t) - \hat{r}(f, z))^2, \quad (6)$$

where  $N_{t,z}$  indicates the total number of measurements across times and stations at depth  $z$ .

In Figure 2 we show the distribution at 1 Hz of the  $r_i(1, t; z_i)$  and  $v_i(1, t; z_i)$  as a function of depth with the violin plots, while the means,  $\hat{r}(1; z)$  and  $\hat{v}(1; z)$  are indicated with orange points. The median across depths and times, as opposed to the mean, is shown in red. The black bars indicate the 16th and 84th percentiles of the distributions shown in blue.

NOTES:

- I have a table with all of the mine blasts and what data we use from them. I can add this trivially.
- I have not included a plot showing the radial-to-vertical phase and a time-trace, but I also have that plot handy.
- I am not sure how much detail to include at the moment. Do we have a target journal? I had the impression we wanted to keep things relatively short.

## B. Markov Chain Monte Carlo Estimation of Model Parameters

(need to motivate bi-exponential model properly.) The plots in Figure 1 show a distinctive shape that can be fit by a bi-exponential model. In [1] the authors construct a model for the fundamental R-wave eigenfunction based on a power-law velocity depth profile for S-waves. They fit a bi-exponential model to the R-wave eigenfunction for many different theoretical power-law velocity depth profiles and Poisson ratios and calculate the mean and standard deviation of the parameters in those fits. For this model, the parameters of the bi-exponential model are independent of frequency, although this need not necessarily be true. [add a source for this statement?](#)

We use our measurements to estimate the parameters in the bi-exponential fits to the radial and vertical data points. We use  $m_R$  and  $m_V$  to refer to the bi-exponential models for the radial and vertical eigenfunctions, and these models depend on a set of intrinsic model parameters,  $\vec{\theta}$ , the depth,  $z$ , and the frequency,  $f$ . We define the  $m_R$  and  $m_V$  as

$$m_R(f, z; \vec{\theta}) = \left( e^{-2\pi f z \frac{a_1}{c_R(f)}} + c_2 e^{-2\pi f z \frac{a_2}{c_R(f)}} \right) \times \frac{1}{1 + c_2} \quad (7)$$

$$m_V(f, z; \vec{\theta}) = \left( e^{-2\pi f z \frac{a_3}{c_R(f)}} + c_4 e^{-2\pi f z \frac{a_4}{c_R(f)}} \right) \times \frac{N_{vh}}{1 + c_4}. \quad (8)$$

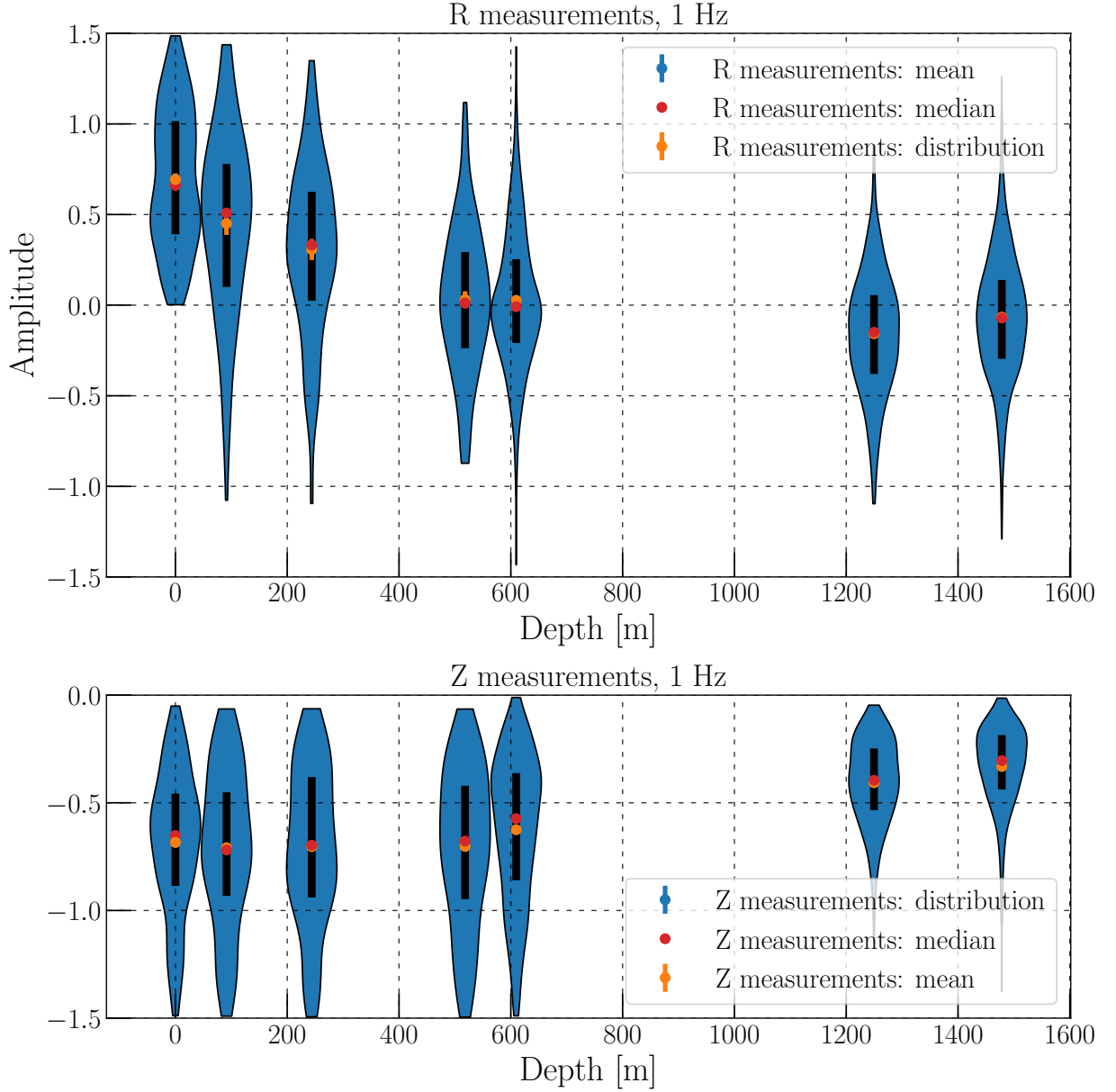


FIG. 1: (fill me, update plot with notation from text. Plot needs a slight modification...need to fix orange point on surface to be 1.)

These functions can be compared to  $r_1$  and  $r_1$  in [1]. Below, we estimate the parameters in the bi-exponential model,

$$\vec{\theta} = (N_{vh}, c_2, c_4, a_1, a_2, a_3, a_4),$$

using the data,  $\hat{v}(f, z)$  and  $\hat{r}(f, z)$ . The assumption that the  $c$ 's and the  $a$ 's do not change with frequency is intrinsic to the theoretical model outlined in [1] and could, in principle,

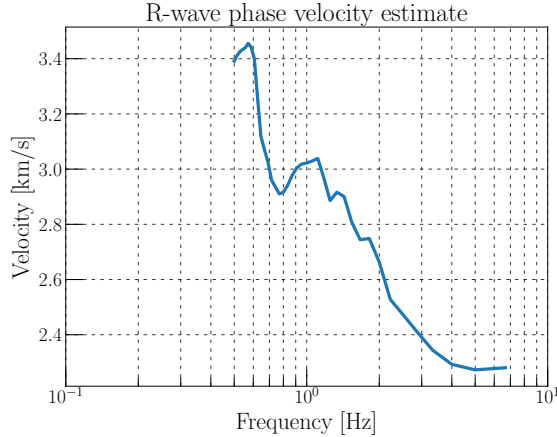


FIG. 2: Estimate of phase velocity as a function of frequency obtained from ambient noise correlations at the 3D Homestake seismometer array. **not sure how else to cite this...Daniel is it possible to cite Daniel's thesis? Feel free to add comments on updates to plot itself as needed.**

be relaxed.

**this paragraph may be better in previous section** The phase velocity dispersion curve for R-waves,  $c_R(f)$ , is estimated using ambient noise correlations. A plot of  $c_R(f)$  is shown in Figure 2.

We use the `MultiNest` package [2] to perform a Markov chain monte carlo (MCMC) analysis to estimate the parameters,  $\vec{\theta}$ . `MultiNest` is commonly used in the astrophysics community, is designed to efficiently sample multimodal distributions and large parameter spaces, and offers robust Bayesian evidence estimates. The posterior probability distribution we use `MultiNest` to explore is given by

$$p(\vec{\theta}|\{\hat{r}, \hat{v}\}) = \frac{p(\{\hat{r}, \hat{v}\}|\vec{\theta})p(\vec{\theta})}{\int d\vec{\theta} p(\{\hat{r}, \hat{v}\}|\vec{\theta})p(\vec{\theta})}. \quad (9)$$

The likelihood function,  $p(\{\hat{r}, \hat{v}\}|\vec{\theta})$ , is taken to be a Gaussian

$$\ln p(\{\hat{r}, \hat{v}\}|\vec{\theta}) = -\frac{1}{2} \sum_f \sum_z \left( \frac{[\hat{r}(f, z) - m_R(f, z; \vec{\theta})]^2}{\sigma_r^2(f, z)} + \frac{[\hat{v}(f, z) - m_V(f, z; \vec{\theta})]^2}{\sigma_v^2(f, z)} \right). \quad (10)$$

We assume that the prior probability distribution,  $p(\vec{\theta})$ , can be split into the product of independent Gaussian prior probability distributions on each individual parameter. We

use [1] to inform the Gaussian prior probability distributions. The definition of our parameters differ slightly from those in [1], but we can generate prior information on each parameter using some combination of information from that manuscript. We also widen the uncertainty on those parameters enough to allow for sufficient exploration of the parameter space, given that our situation is likely different from the theoretical one considered in [1].

The results of the parameter estimation, along with the prior information on each parameter, is summarized in Figures 3 and 4 and Table I.

Figure 3 shows that the model fits the data reasonably well across all frequencies used in the analysis. Figure 4 shows that there is very little difference between the prior and posterior distributions, which implies that the measurements generally agree with the theoretical predictions. [expand this discussion](#)

These measurements represent the first explicit estimate of the depth dependence of the R-wave eigenfunctions using a three-dimensional seismometer array.

Parameter	Mean	Error	Prior Mean	Prior Error
$c_2$	-0.76	0.06	-0.8	0.1
$a_1$	0.86	0.06	0.85	0.1
$a_2$	0.63	0.06	0.7	0.1
$c_4$	-0.69	0.07	-0.74	0.1
$a_3$	0.49	0.06	0.7	0.4
$a_4$	0.81	0.1	0.8	0.2
$N_{vh}$	-0.68	0.02	-0.6	0.2

TABLE I: [values in table need to be updated](#) Results for R-wave eigenfunction parameter estimation. We show estimates and uncertainty for the parameters from the 1-dimensional marginalized posterior distribution on each parameter. We also show the mean and standard deviation of the Gaussian prior probability distribution used for each parameter.

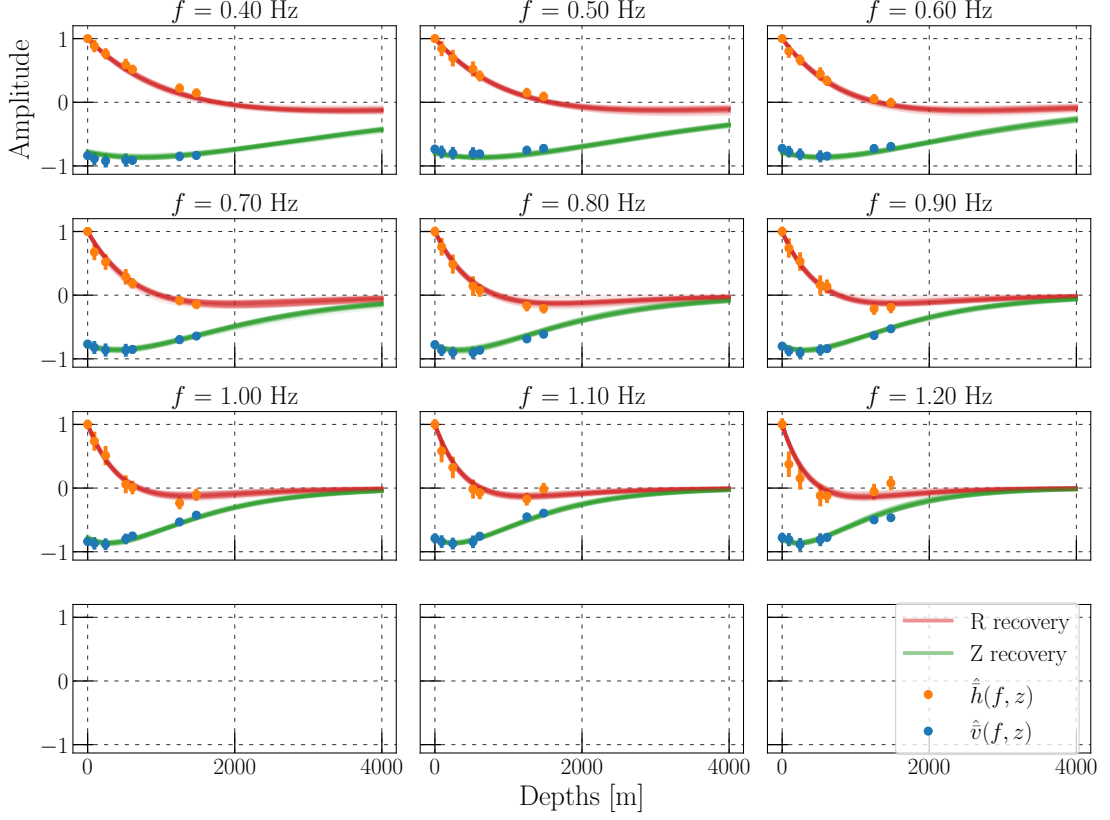


FIG. 3: Rayleigh-wave parameter estimation fits for all of the data used. The red and green curves are examples of the bi-exponential models evaluated at parameters whose values are generated with random draws from the posteriors presented in Figure 4. The width of those lines is proportional to the range of values at each depth one might expect the R-wave eigenfunction to take given the parameter estimation we have performed and the model we have used. The orange points are the data supplied to the sampler. That is, the orange points correspond to  $\hat{r}(f, z)$  and the blue points correspond to  $\hat{v}(f, z)$ .



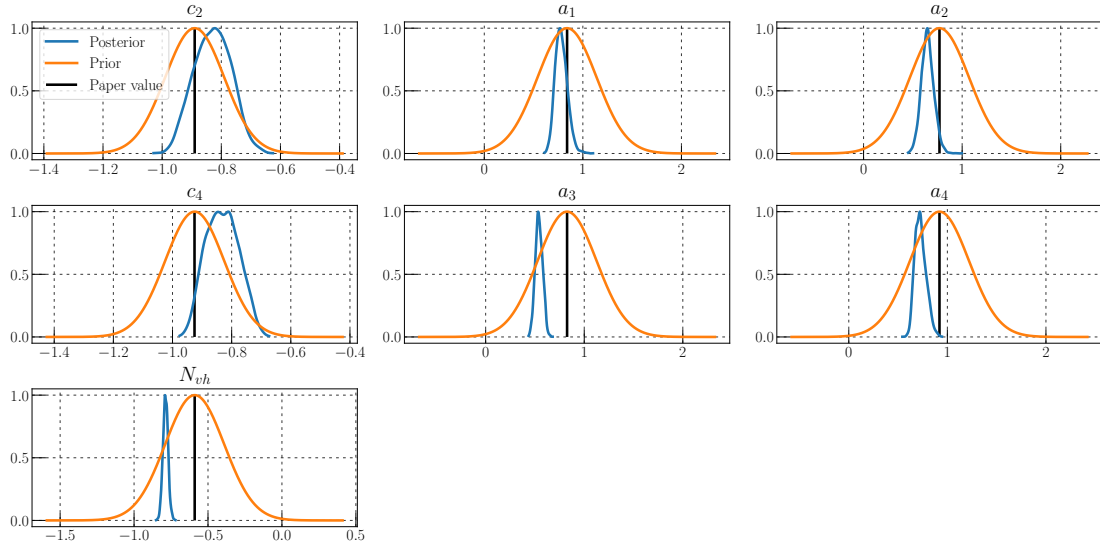


FIG. 4: fill me.

### III. RESULTS: OBSERVATIONS AND MODEL ESTIMATES

### IV. CONCLUSIONS

#### References

- 
- [1] Matthew M Haney and Victor C Tsai. Nonperturbational surface-wave inversion: A Dix-type relation for surface waves. *GEOPHYSICS*, 80(6):EN167–EN177, November 2015.
  - [2] F Feroz, M P Hobson, and M Bridges. MultiNest: an efficient and robust Bayesian inference tool for cosmology and particle physics. *Monthly Notices of the Royal Astronomical Society*, 398(4):1601–1614, October 2009.